Nuclear Instruments and Methods in Physics Research B 549 (2024) 165263

Contents lists available at ScienceDirect

Nuclear Inst. and Methods in Physics Research, B

journal homepage: www.elsevier.com/locate/nimb

Positron-annihilation lifetime spectroscopy with in-situ control of temperature, pressure and atmosphere to determine the free-volume of soft materials

R. Helm [a,*], J. Lehtonen [a], M. Mayerhofer [a], J. Mitteneder [a], W. Egger [a], R. Verbeke [b], P. Sperr [a], G. Dollinger [a], M. Dickmann [a]

[a] Institute for Applied Physics and Metrology, University of the Bundeswehr Munich, Neubiberg, Germany
[b] Membrane Technology Group, Centre for Membrane Separations, Adsorption, Catalysis and Spectroscopy for Sustainable Solutions (cMACS), KU Leuven, Leuven, Belgium

ARTICLE INFO

Keywords:
Positron-annihilation lifetime spectroscopy
Free-volume determination
Polymer plasticization
Porosimetry

ABSTRACT

We introduce a newly developed instrument for ^{22}Na-based positron-annihilation lifetime spectroscopy (PALS) with in-situ temperature, pressure and atmosphere control. The system is designed for PALS measurements of samples in changing atmospheric conditions, from vacuum ($\sim 10^{-5}$ mbar) up to a gas pressure of 20 MPa. Furthermore, we can select the composition of the applied gas, such as N_2, Ar, Ar/H_2, CO_2 as well as CH_4 and adjust the sample temperature from room temperature to 200 °C. To test the measurement principle, we carried out PALS measurements on semi-crystalline polystyrene in (99.999 %) pure argon atmosphere varying the pressure and the temperature simultaneously, up to 4 MPa and T = 150 °C. Changing the sample environment in that way affects the free-volume of the polymer, which is reflected in the positron lifetime and intensity.

1. Introduction

During the last decades, the development of new polymer and membrane materials for various environmental, energy and medical applications has gained importance [1], e.g. gas-separation [2], carbon capture [3], water purification [4,5] and reverse osmosis [6]. An important property of these polymer materials is the free-volume (V_F), i.e. the difference of the macroscopic volume (V) and the temperature and pressure independent volume occupied by the polymer molecules (V_{occ}). The V_F consists of free-volume elements (FVEs) that originate from irregular packing in the glassy state (*static* FVEs) or from segmental motion in the rubbery state (*dynamic* FVEs) [7]. Sometimes the fractional free-volume V_F/V, the ratio between free volume and macroscopic volume, is used to characterize the free-volume in polymers [8].

According to the free-volume theory [8,9], the V_F is responsible for the transport of atoms or molecules in and through the polymer matrix. Accordingly, the transport mechanisms are strongly governed by the FVEs size and distribution, the size of the penetrating atoms or molecules, as well as their interactions [2,10]. For example, the size of the FVEs in ion-exchange membranes determines the size of the molecules that can be transported across the membrane [4]. The size of V_F depends mainly on the thermodynamic state of the system, i.e. temperature and pressure [10], but is also specific for each polymeric system. In the glassy state of polymers, the molecule chains are rigid and the effect of temperature on V_F is scarce. When reaching the glass transition temperature T_g the polymer chains begin to soften and the FVEs expansion accelerates with increasing temperature [11]. Softening of polymer chains may also be due to the presence of an atmosphere, e.g. humidity, gases or gas mixtures, and its pressure. The process of softening the polymer chains by a penetrant gas is known as plasticization and is a function of the gas solubility in the polymer and the pressure of the atmosphere [12]. In addition, varying ambient conditions can cause changes in the polymer structure, which leads to a change in the transport of molecules through the polymer matrix [10]. To obtain more insight on the size and abundance of the FVEs, positron-annihilation lifetime spectroscopy (PALS) has been used.

PALS is a reliable, nondestructive analytical method often used for the characterization of FVEs in the range of 1–30 Å [13,14]. With this technique, the lifetime of positrons in matter is determined by measuring the radiation caused by the annihilation of a positron with an

* Corresponding author at: Werner-Heisenberg-Weg 39, 85577 Neubiberg, Germany.
E-mail address: ricardo.helm@unibw.de (R. Helm).

https://doi.org/10.1016/j.nimb.2024.165263
Received 7 September 2023; Received in revised form 12 January 2024; Accepted 26 January 2024
Available online 2 February 2024

electron. The positron lifetime is the elapsed time between the implantation of the positron into the material and the detection of at least one gamma emitted by the annihilation. It depends on the electron density at the location of annihilation. Thus, it is characteristic for different materials and their atomistic defects. Consequently, the lifetime of the positron increases when the local electron density decreases, which translates directly to the dimension of the defect.

In most polymers, a bound state of e^+ and e^- can form, the Positronium (Ps). Positronium exists in two spin states, i.e. *para*-Positronium (p-Ps) with s = 0 and *ortho*-Positronium (o-Ps) with s = 1, the latter most likely annihilates into three photons in vacuum. While the mean vacuum lifetime of p-Ps is 125 ps and will not change much in matter, the lifetime of o-Ps can be substantially shorter than its vacuum lifetime of 142 ns. In low electron density environments, e.g. polymer materials, o-Ps can annihilate with another surrounding electron that satisfies the selection rule of an s = 0 state, resulting in a process called "pick-off" annihilation, which reduces the o-Ps lifetime to nanoseconds [15–17]. This reduced o-Ps lifetime yields information about size or size distribution of V_F in polymer materials.

It is well-established that the size of FVEs in polymers usually increases with temperature, which can be observed in the increase of o-Ps lifetime [18–22]. Measurements of various polymer materials show that, for specific gases, the lifetime of o-Ps increases with increasing pressure, but decreases after a certain point [23].

Usually only one of the two parameters (temperature, pressure) is changed during the measurement, while the other technically easy-to-set conditions (air/vacuum, room temperature) are kept constant. For many polymers, however, these measurement conditions are insufficient to elucidate the material structure-performance relationship under actual operation, such as for pressure-driven membrane applications. Yet, very few studies show the influence of gas pressure or gas species while simultaneously varying temperature on the o-Ps lifetime in polymers and therefore, on the FVEs [23,24]. Here, we introduce a new instrument that is capable of measuring in-situ PALS with independent adjustment of ambient conditions, i.e. temperature, atmosphere and pressure. This instrument exposes the polymer directly to a defined atmosphere and provides information not only on the influence of pressure and temperature, but also on the influence of dissolved gas species on the free-volume of the polymer, resulting in a more realistic experimental environment for polymer materials used in various fields of science and engineering.

2. Apparatus

2.1. General design

A technical drawing of the instrument is shown in Fig. 1a. The apparatus consists of a vacuum section (top) and a high-pressure section (bottom), that can be mechanically separated from one another. The high-pressure unit can be evacuated and flooded with gas after separation from the vacuum unit. A scroll pump (Edwards nXDS10i) and a turbo pump (Edwards EXT70H) are installed at the vacuum section and the whole system is vacuum tight down to at least 10^{-5} mbar. The

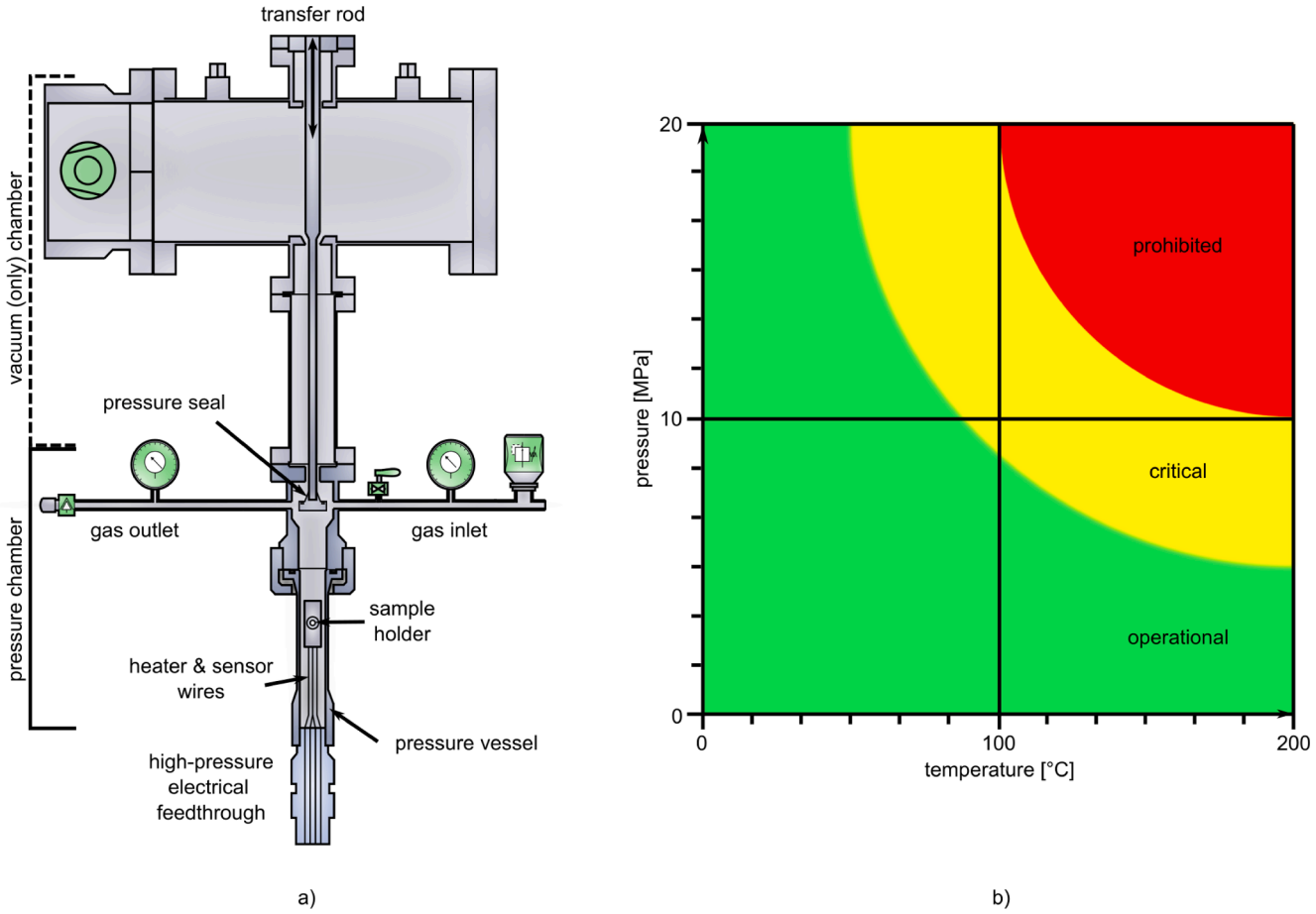

Fig. 1. (color, 2-column): a) A sketch of the basic design of the instrument with all important components. The instrument consists of a high-pressure chamber and a vacuum chamber, both can be mechanically separated by closing the pressure seal. The high-pressure chamber, which is also vacuum-tight, includes the gas circuit, the pressure vessel and the high-pressure electrical feedthrough for heating and temperature monitoring. b) Estimation, based on static thermo-mechanical simulations, of the application range of temperature and pressure for the pressure vessel. The green area shows the parameter space that is unproblematic to set. Parameter combinations in the yellow area should be applied with care and the red area is restricted.

vacuum is essentially limited by the components on the pressure side of the unit and the small turbo pump used, but is sufficient for degassing the samples environment.

In the gas control-circuit, the desired gas or gas mixture can be set and introduced to the pressure vessel. The pressure is monitored with two pressure gauges located near the pressure chamber at the gas inlet and outlet, respectively.

For pressure tightness, the pressure chamber must be isolated from the vacuum reservoir. This is realized by sealing the pressure chamber with a pressure seal. The pressure seal consists of a Viton® gasket on a metal disk which presses on a ring welded into the tube right beneath the undermost vacuum flange. It is operated with a transfer rod from the vacuum side of the instrument (see Fig. 1a). The seal is closed in direction of the pressure gradient from high to low pressure and is therefore self-sealing.

The pressure vessel is designed for up to 20 MPa of gas pressure and temperatures up to 200 °C. Fig. 1b shows a schematic p-T area of application for the instrument. This graph is an estimation based on simulation (Ansys [25], Solidworks [26]) and analytical calculations. The green area shows the pressure–temperature combination that has been extensively tested and is suitable for measurement operation. The yellow area is in principle accessible but has not been fully explored. For pressure–temperature combinations in the red area, safe operation cannot be guaranteed. Calculations of the yield stress of the pressure vessel for the maximum design values of pressure and temperature yielded a maximum stress of 452 MPa before material failure. A thermo-mechanical simulation showed that the maximum stress in the vessel does not exceed 204 MPa under the conditions marked in green and yellow in Fig. 1b. It should be noted that these calculations are for the static case and do not account for any dynamic stress, which can occur during subsequent pressure–temperature cycles.

2.2. Positron source and sample holder

As a positron source, we use ^{22}Na salt encapsulated in 7 μm thick Kapton® foil with an activity of about 370 kBq (10μ Ci), which provides sufficient count rates (31 cps) while minimizing background due to false coincidence events. The positron source was provided by the Martin-Luther-University Halle-Wittenberg. When Kapton® is used for the confinement of the ^{22}Na salt, the maximum allowable temperature must be below 200 °C. The positron source is placed between two identical samples, forming a so-called sample-source sandwich.

In Fig. 2, a detailed description of the sample holder is depicted. The sample holder generally consists of three main components, two jaws

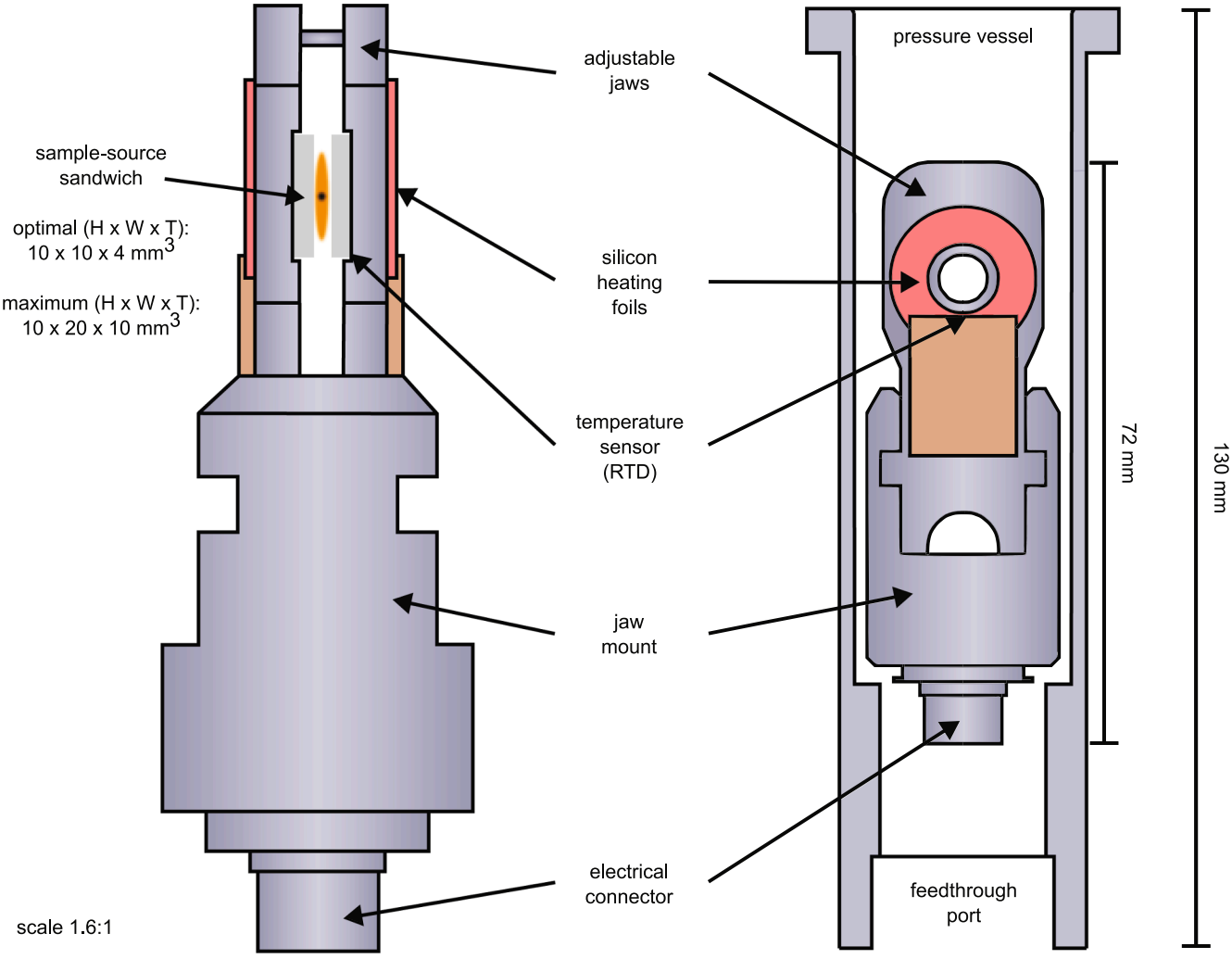

Fig. 2. (color, 2-column): Detailed description of the sample holder. On the left side the sample-source sandwich can be seen placed between the two jaws and mounted onto the jaw mount. The jaws not only hold the sample-source sandwich at a defined position but also act as a thermal conductor between the heating foils and the sample. The heating procedure can be controlled by a resistance temperature detector integrated in one of the jaws. On the right side, the position of the sample holder in the pressure vessel is shown. This position is only obtained if the feedthrough is also installed, but for the sake of clarity the feedthrough was omitted.

and a jaw mount. The sample-source sandwich is placed between two jaws, which holds the sample-source sandwich in place and can be adjusted to fit samples with a maximum thickness of 5 mm per sample (10 mm for the sample-source sandwich). Moreover, the jaws serve as the thermal contact between two mounted silicon heating foils and the sample-source sandwich. Isolated from the heating foils a resistance temperature detector (RTD) is embedded in one of the jaws to control the sample temperature during in-situ heat treatment experiments. The two jaws can be attached via screws to each other and kept in place in guide rail to prevent movement of the sample during the experiment. The jaw mount is connected to a high-pressure feedthrough, which allows for electrical contacting from outside the pressure vessel.

2.3. Data acquisition

The data acquisition concept of the instrument can be seen in Fig. 3. The ambient parameters, i.e. temperature and pressure, can be monitored through the LabVIEW user interface. The annihilation radiation is detected by two detectors from SCIONIX. The detectors consist of two Hamamatsu R13089-100 photomultipliers (PMT) [27] each mounted with a 25 mm thick encapsulated $CeBr_3$ scintillator crystal. The detector signals are digitized by the DRS4 evaluation board, a digital oscilloscope developed by the Paul-Scherrer Institute in Switzerland [28], which is already used by other research groups for PALS [29,30]. To evaluate the annihilation events and extract the positron lifetime we use the DDRS4PALS, a software developed for the positron-annihilation lifetime spectroscopy with the DRS4 board that offers a wide variety of digital filters to optimize the quality of the acquired lifetime spectra, e.g. timing resolution and peak-to-background ratio [31]. For the analysis of positron annihilation lifetime measurements, the knowledge of the timing resolution of the data acquisition is critical. In the lower right corner of Fig. 3, the prompt spectrum for 511 keV gamma events can be seen. Since both 511 keV gamma quanta are measured and they are generated simultaneously, the time difference (width of the spectrum) is only due to the time inaccuracy of the electronics, detectors and scintillators. Fitting of the prompt spectrum yields the time resolution of the system and could be determined to be 313(3) ps (FWHM). Assuming identical characteristics of the photomultipliers, the single detector timing resolution can be approximated to be 221(2) ps (FWHM).

For proper data analysis, a minimum of 2×10^6 events/spectrum (17 h) for polymer materials and 4×10^6 events/spectrum for metals and semiconductors are required. These values are empirical values and have proven to be sufficient in numerous experiments in the past. To extract the instrument resolution function at each pressure level, a p-type Silicon reference sample with 4×10^6 events/spectrum was measured before every measurement series.

Although not addressed in this work, it is generally possible to install different detector systems to measure different parameters of positron annihilation, e.g. the energy distribution of the annihilation radiation, which can be used to measure Doppler Broadening Spectroscopy (DBS) when measured separately, or Age Momentum Correlation (AMOC) when measured simultaneously with positron lifetime [32].

2.4. Positron-Lifetime Annihilation Spectroscopy (PALS)

PALS measurements are performed utilizing the positrons from the

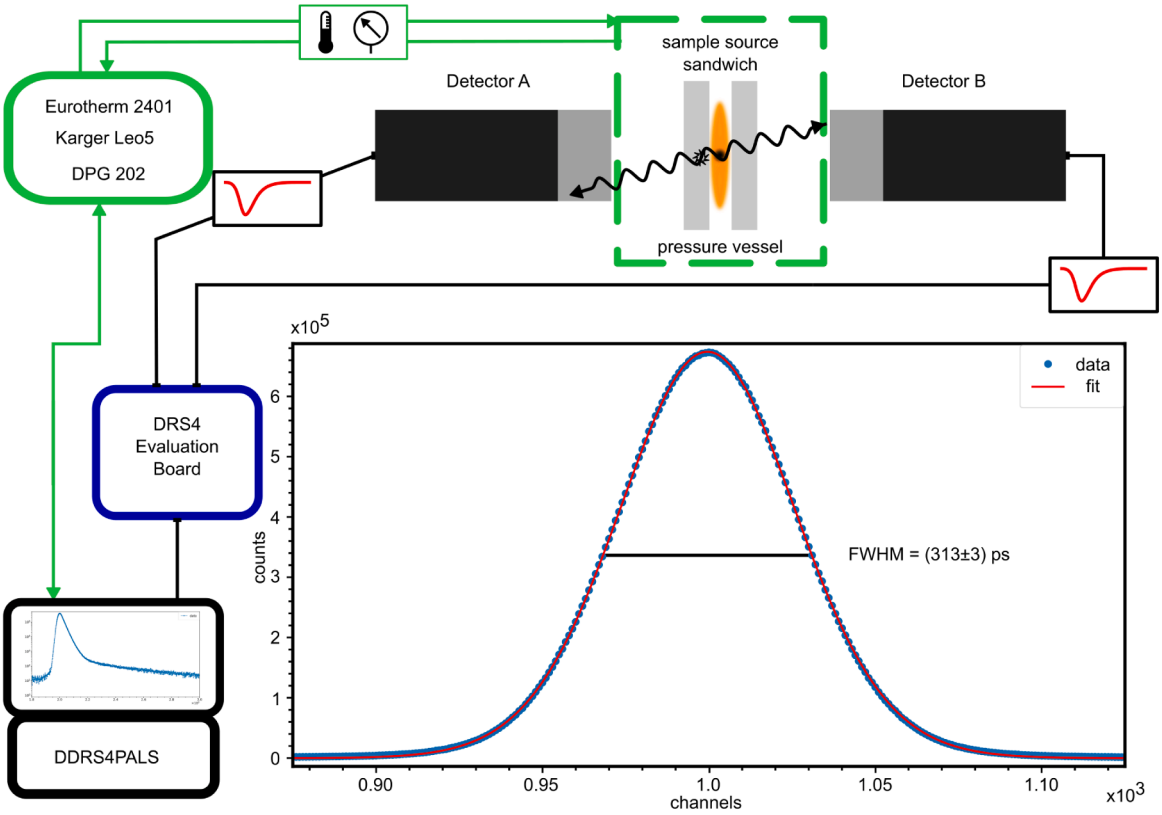

Fig. 3. (color, 2-column): Schematic of the data acquisition unit. Both gamma events, i.e. start and stop events, are registered by the PMTs. The resulting anode signals (black circuit) are directly delivered to the analogue input of the DRS4 evaluation board [28] and processed by DDRS4PALS software [31]. The ambient parameters (green circuit) are monitored by a LabVIEW user interface. The graph in the lower right corner is a so-called prompt spectrum for 511 keV gamma events. By fitting a gaussian-like function to the data, we can analyse the width (FWHM) of the prompt spectrum, which corresponds to the instrument time resolution of the spectrometer for 511 keV gamma events.

β^+-decay of the ^{22}Na source. The positron emission is directly followed by the emission of a gamma (1.27 MeV) of the daughter nuclei ^{22}Ne, thus, the detection of this gamma serves as the start of the positron that is directly implanted into the material of interest. The electron–positron annihilation inside the material emits in most cases two 511 keV photons that are used to detect the end of the positron lifetime. Therefore, the lifetime of the positron is evaluated by the time difference of the 1.27 MeV and the 511 keV signals taken in coincidence for each annihilation event. A PALS-spectrum is obtained by collecting the number of annihilation events for each bin of positron lifetimes, resulting in a time-dependent spectrum $D_{exp}(t)$ like the on depicted in Fig. 4. The measured distribution is well modelled by a function $D_{mod}(t)$, a sum of exponential functions convoluted with an instrument resolution function $IRF(t)$ and superimposed on a background B:

$$D_{mod}(t) = IRF(t) * \left(\sum_{i=1}^{k} \frac{I_i}{\tau_i} \exp\left(-\frac{t}{\tau_i} \right) \right) + B \tag{1}$$

where k is the number of resolvable exponentials and I_i the relative intensity of the i-component in the spectrum. τ_i represents the mean decay time that corresponds to the mean lifetime of a subpopulation i of the positrons that experience a similar electron density in the material.

3. Results and discussion

The thermoplastic polystyrene (PS) was the first polymer system for which simultaneous gas pressure and temperature-dependent PALS measurements were performed with the new instrument. The reason for this choice is that the glass transition temperature (T_g) of PS is around 97 °C [33] and therefore, is significantly above room temperature and in the middle of the feasible temperature range of the instrument. This means that sufficient temperature points can be collected before and after the T_g without the necessity of sample cooling below room temperature. Compared to other thermoplasts, e.g. PMMA or PVC, with similar glass transition properties, PS possesses a higher gas diffusion constant D(30 °C) = 7.5×10^{-8} cm^2 s^{-1} for the penetrant argon [34,35]. Diffusion in polymer materials is mainly governed by the atomic radius of the penetrating gas species [8,10,34]. Therefore, argon is a suitable penetrant due to its small atomic radius of d_{Ar} = 0.279 nm, its inert chemical nature and accessibility [35,36]. The PS was purchased from Sigma-Aldrich as a semi-crystalline sheet with a dimension of 300 × 300 mm^2 and a thickness of 2 mm. Two 10 × 10 mm^2 pieces were cut out of the sheet and the positron source was placed in between the pieces (cfr. sample-source sandwich). The maximum energy of the positrons emitted by the ^{22}Na source is 0.546 MeV. The implantation of the positron into the material can be described by a power law of the following form [32]:

$$P_+(z) = \alpha \exp(-\alpha z), \alpha\left[\mathrm{cm}^{-1}\right] = 17 \frac{\rho[\mathrm{g/cm}^3]}{E_{max}^{1.43}[\mathrm{MeV}]} \tag{2}$$

This implantation profile $P_+(z)$ in the direction perpendicular to the sample surface is mainly dependent on the density ρ and the maximum positron energy E_{max}. In Fig. 5 the implantation profile from Eq. (2) is shown for silicon (ρ = 2.33 g/cm^3), PS (ρ = 1.05 g/cm^3) and silica aerogel (ρ = 0.35 g/cm^3) for a maximum sample thickness of 2 mm. The maximum penetration depth, i.e. when the implantation profile decreased to zero, changes with the density from 0.5 mm (silicon) to 4 mm (silica gel). The calculation of the implantation profile for PS with a density of 1.05 g/cm^3 and a maximum positron energy of 0.546 MeV shows that a sample thickness of 2 mm is sufficient to avoid positrons escaping the sample material and annihilation elsewhere. For the pressure measurements, commercially available argon with a purity of more than 99.999 % was used as the penetrant gas.

3.1. Room temperature measurements on polystyrene (PS)

Fig. 4 shows the spectrum of polystyrene at 0.1 MPa argon pressure and room temperature. The blue dots represent the raw data points that are not considered in the data analysis. The green dots show the data points which are used by the fit routine of Eq. (1) (black solid line). The red dotted horizontal line displays the mean background of the spectrum. The evaluated lifetime spectra contain three lifetime components, $\tau_1 \approx 125$ (fixed) ps (blue dashed line) can be attributed to the annihilation of p-Ps, while τ_2 = 388(2) ps (orange dashed line) stems from free positrons annihilating directly in the polymer matrix, without forming positronium. The third component τ_3 = 2056(3) ns (green dashed line) can be associated with the pick-off annihilation of o-Ps close to the walls of the FVEs. All spectra analyzed showed the best results when 3 components were used for the model of Eq. (3). For small FVEs (r < 1 nm) the Tao-Eldrup model [37,38], based on the assumption of spherical or cylindric FVEs, was used as an approximation between the lifetime τ_3 and the mean radius of the FVEs:

$$\tau_3 = \frac{1}{2}\left[1 - \frac{r}{r + \Delta R} + \frac{1}{2\pi}\sin\left(\frac{2\pi r}{r + \Delta R}\right)\right]^{-1} \text{ns} \tag{3}$$

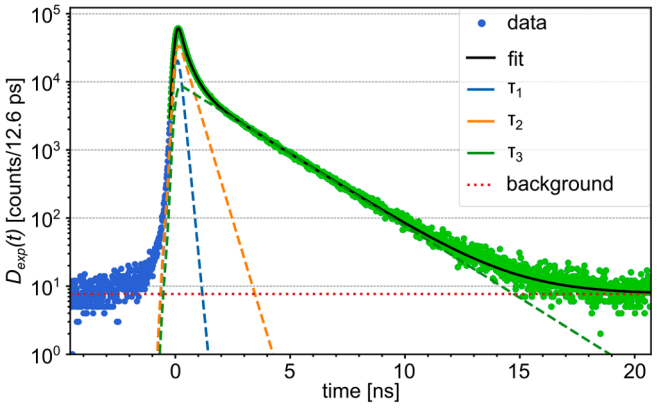

Fig. 4. (color, 1-column): Fitted decay spectrum of polystyrene at room temperature and 0.1 MPa argon atmosphere. The raw data points are represented in blue and green: The data points that are included in the fitting process are printed in green, the ones in blue are not considered in the fitting process. Indicated in dashed lines are the exponential components attributed to the different positron lifetimes resulting from the least-square fit of the function from Eq. (1).

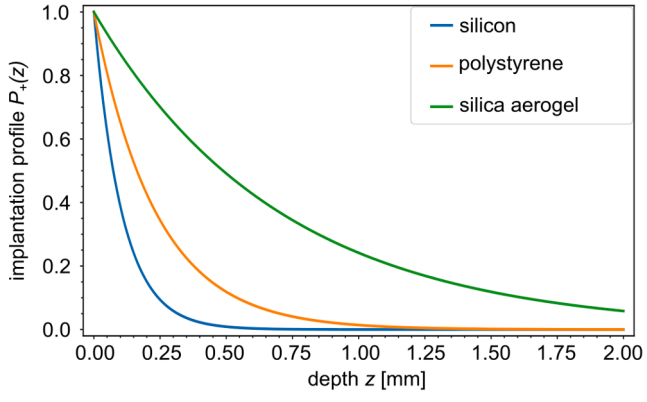

Fig. 5. (color, 1-column): Calculations of the implantation profile $P_+(z)$ with Eq. (2) for three different materials for a maximum sample thickness of 2 mm. It shows the dependence of the positron implantation on the density of the material. Silicon (ρ_{Si} = 2.33 g/cm^3) exhibits the least implantation distance of 0.5 mm, followed by polystyrene (ρ_{PS} = 1.05 g/cm^3) with 1.3 mm and silica gel ($\rho_{silicagel}$ = 0.35 g/cm^3), where a sample thickness of 2 mm would not be sufficient. This must be considered to prevent positrons from escaping the sample and annihilating elsewhere.

The empirically determined parameter ΔR approximates the reduction of the FVE radius due to interactions between o-Ps and electrons of the surrounding polymer chains. The value of ΔR was determined to be 0.166 nm by calibration measurements on several molecular solids [14,37,38]. Although for larger FVEs ($r > 1$ nm), the Tao-Eldrup model insufficiently correlates τ_3 with the radius of the FVEs, it is well applied for the measured positron lifetimes in PS, where the mean radii of the FVEs are below 1 nm. In any case, the model could be extended to account for the 3 γ annihilation, which becomes increasingly probable as the size of V_F increases and τ_3 approaches the vacuum lifetime of o-Ps [39]. The resulting mean positron lifetime of 2056(3) ns corresponds to a mean radius of the FVEs of the PS of $r = 0.2899(3)$ nm at room temperature and 0.1 MPa argon pressure, meaning that it is well in the validity range of the Tao-Eldrup model (Eq. (3)).

3.2. Temperature dependent measurements on PS

During the first test for temperature dependent measurements, the thermal contact between the sample and the heating element was tested. Therefore, we heated the sample in air and measured the sample temperature at three different locations T_{s1}, T_{s2} and T_c. Thermocouples were positioned on either side (T_{s1}, T_{s2}) and in the center (T_c) of two 10 × 10 × 2 mm^3 polychlorotrifluoroethylene (PCTFE) sheets. The thermocouples on the sides of the PCTFE stack are thermally isolated from the jaws, to eliminate measurement distortion. We then calculated the mean temperature across the two PCTFE sheets. The slope of the linear fit of mean sample temperature and the set temperature was determined to be 0.98(0.01) over the range from 23(3) °C up to 200 °C. This shows sufficient thermal contact of the heating element to the sample and reveals a temperature difference of 2(1) % from the outside to the center of the polymer stack. It is important to mention that this difference can change for different materials. However, since the thermal conductivity coefficient of most polymers is rather low and in the same order of magnitude, the influence on the measurement are similar and negligible [40]. The samples were heated from room temperature 21(2) to 150(3) °C in increments of 25 °C and for every temperature a positron-annihilation lifetime spectrum was recorded.

Fig. 6 shows the temperature dependence of τ_3 and I_3 in 0.1 MPa argon atmosphere. For spatial reference, the FVE radius was calculated with Eq. (3) and is shown on the right-hand y-axis. The glass transition temperature (T_g) is depicted as a dashed vertical line. The lifetime analysis gives an o-Ps lifetime τ_3 of roughly 2 ns with an intensity I_3 of 0.4 %. The lifetime τ_3 is an indicator for the dimension of the FVEs and I_3 for the abundance of the FVEs. The results of the temperature dependence of τ_3 and I_3 are shown in Table 1. At temperatures below the T_g the increase in τ_3 is less than 200 ps. Above the T_g, a steeper increase in τ_3 is noticeable (≈500 ps/50 K), while the intensity I_3 of this component increases only from 0.41 to 0.42 between 100 °C and 150 °C. Below the T_g, PS is in a non-equilibrium, glassy state, where the polymer chains minimal segmental mobility and the increase in τ_3 with increasing temperature is marginal. When the temperature reaches the T_g, i.e. upon the phase transition from glassy to rubbery, the polymer chains become more mobile and τ_3 increases more rapidly due to the increasing temperature. The negligible

Table 1
o-Ps lifetimesτ_3 and intensities I_3 of PS as a function of temperature and 0.1, 2 and 4 MPa argon pressure. The statistical uncertainty of I_3 from the fit is below 0.001 and is therefore omitted.

T [°C]	21(2)	50(1)	75(2)	100 (2)	125 (3)	*140 (3)** 146 (2) 150(3)	
p = 10^{-9} MPa	2021 (5)	2064 (5)	2122 (5)	2283 (5)	2475 (5)	**2731 (5)	τ_3[ps]
	36.3	38.2	38.4	42.6	43.6	**43.7	I_3[%]
p = 0.1 MPa	2056 (3)	2077 (5)	2135 (5)	2239 (5)	2450 (5)	2724(6)	τ_3[ps]
	40.9	41.5	41.7	42.0	42.3	42.8	I_3[%]
p = 2 MPa	2099 (5)	2168 (6)	2228 (5)	2290 (5)	2448 (5)	2698(5)	τ_3[ps]
	39.4	41.3	41.7	42.0	43.0	43.1	I_3[%]
p = 4 MPa	2183 (6)	2260 (6)	2313 (6)	2400 (6)	2606 (6)	*2724(6	τ_3[ps]
	38.5	41.0	41.8	41.9	42.8	*43.4	I_3[%]

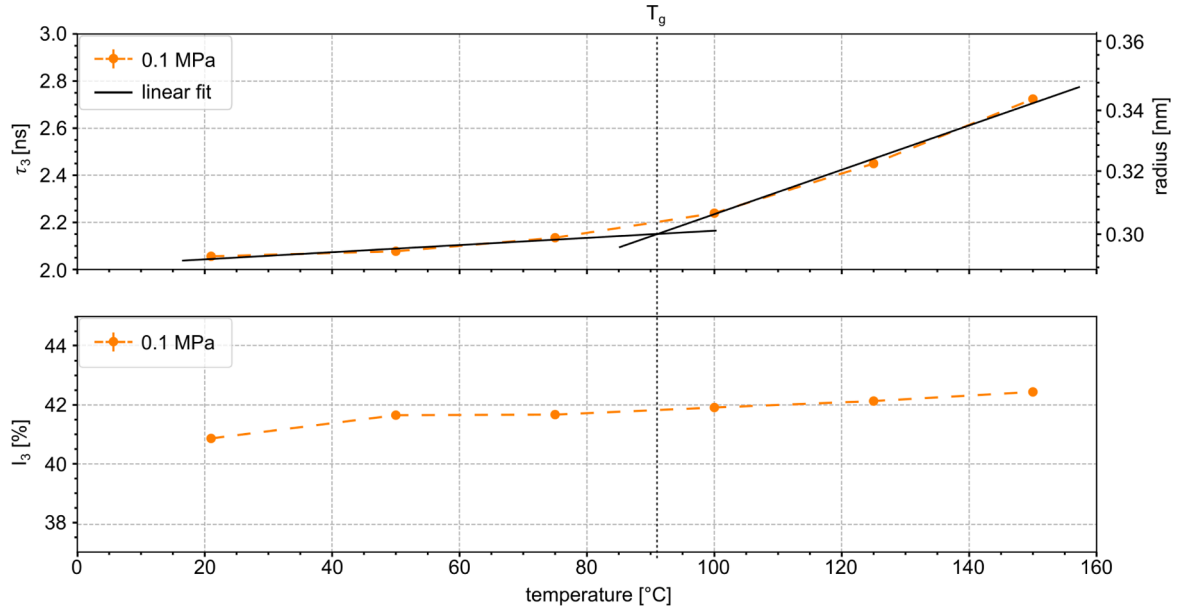

Fig. 6. (color, 2-column): Positron-annihilation lifetime results of the o-Ps lifetime τ_3 and the intensity I_3 of PS at 0.1 MPa as a function of temperature. The corresponding free-volume element (FVE) radius, using Eq. (3), is plotted on the second axis as a geometric reference. There is a clear difference in FVE growth below and above T_g. By linear fitting of these two regions the T_g can be estimated to be 91(5) °C.

temperature dependence of I_3 indicates that at temperatures above the T_g, the FVEs increase in size but not in abundance. Moreover, by linear fitting of the two data regions of τ_3 below and above the T_g, we can estimate the glass transition temperature of PS to be at 91(5) °C (see Fig. 6). The obtained results from the lifetime evaluation are consistent with previous publications [21,41]. In these publications the T_g was determined by means of differential scanning calorimetry (DSC) and positron-annihilation lifetime spectroscopy.

3.3. Pressure dependence of τ_3

In addition to temperature, the influence of the gas pressure on the FVEs of PS was simultaneously measured.

In a first step, we determined the pressure decrease in the pressure vessel at room temperature over a period of 9 days. In that period, the pressure dropped from 13.7(0.5) MPa to 13.5(0.5) MPa. Considering that a measurement with 2×10^6 events/spectrum takes less than 2 days, the pressure loss of approximately 0.02 MPa/day is negligible and can be fully compensated by careful adjustments at the gas-inlet.

For our first test measurements, we investigated the influence of temperature and gas pressure on the V_F of PS. For this purpose, PALS measurements were taken on PS samples as a function of the temperature at vacuum (1×10^{-9} MPa) and 3 different argon pressures: 0.1 MPa, 2 MPa and 4 MPa (see Table 1). Fig. 7 shows the o-Ps lifetime for the four different pressure states as a function of the temperature. On the right-hand y-axis, the FVE radius is displayed as a size reference. At room temperature, τ_3 increases with pressure. Upon heating, the τ_3 (T) curve shifts towards higher lifetimes with increasing pressure. In the glassy phase, there is a comparable increase in V_F concerning temperature in low-pressure (in vacuo, 0.1 MPa) and high-pressure measurements. In the rubbery phase, above the T_g, a steeper increase of τ_3 for lower pressures is apparent. Among all the pressure states measured, the vacuum measurement shows the lowest intensity I_3 below the T_g with a transition to the highest intensity above the T_g. For the measurements in argon atmosphere, a pressure dependence of I_3 below 75 °C is visible, until the intensities of the different pressure states converge at temperature above 75 °C and display an increase for higher gas pressures. The lowest I_3 is reached for 4 MPa and 21(2) °C followed by the 2 MPa and 0.1 MPa measurement, respectively. In Fig. 8 the intensities (I_1, I_2, I_3) for the 2 MPa measurement are shown as a function of temperature. Although I_1 does not show any dependence on temperature or pressure, I_2 and I_3 display an inverse correlation. This inverse correlation holds true for 0.1 MPa and 4 MPa as well.

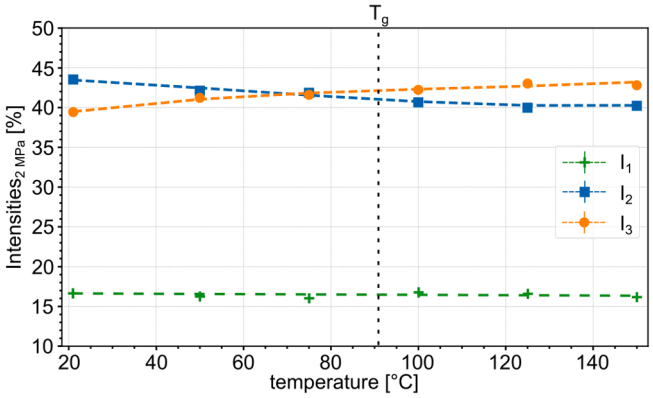

Fig. 8. (color, 1-column): Intensities as a function of temperature for 2 MPa argon pressure. I_1 seems unchanged over the hole temperature range and independent of the phase change. For the intensities I_2 and I_3 an inverse correlation can be observed. The change in the glassy phase can either be explained by [44] or by employing the dual-mode sorption model. In the latter, a temperature dependent gas population can trap in the static FVEs present in the glassy phase. This results in a decrease in o-Ps annihilation and an increase in positron annihilation within the polymer matrix.

The increase in o-Ps lifetime with increasing argon pressure suggests the occurrence of polymer chain reorganization due to the interaction with the argon. Plasticization by argon has indeed been observed for polydimethyl siloxane and poly(ethyl methacrylate), even if argon has a low solubility [33,42,43]. The FVE expansion with increasing pressure is observed in both the glassy state and the rubbery state.

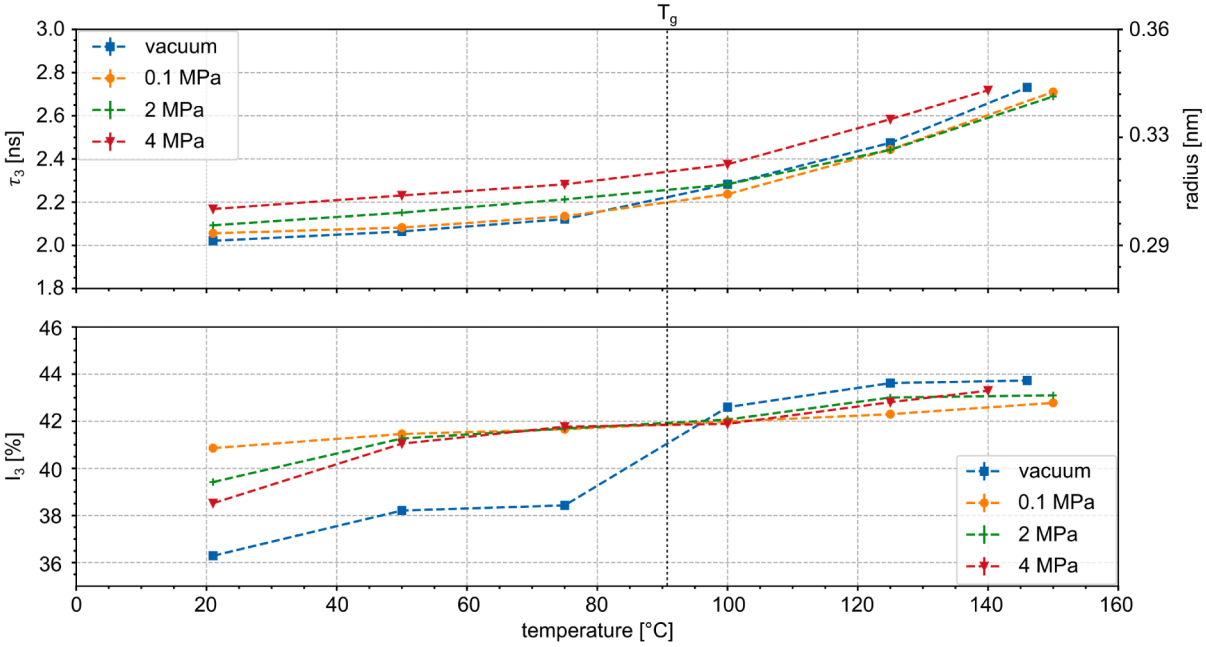

Fig. 7. (color, 2-column): o-Ps lifetime and intensity I_3 of polystyrene at four different pressures. The T_g at 0.1 MPa is marked as a reference point of the phase transition. With increasing argon pressure an offset to higher o-Ps lifetimes is evident. At higher pressures the growth behaviour of the FVEs is similar to that at 0.1 MPa. An opposite trend in the intensity I_3 is present for temperature close to room temperature, which however vanishes at higher temperatures. In vacuum condition the intensity is the lowest in the glassy state and the highest in the rubbery phase with an abrupt transition at the T_g.

In the rubbery phase, the steeper increase of τ_3 with temperature at lower pressures could be explained by the weaker compressive force of the argon on the polymer. In the rubbery phase with increasing gas pressure, the counter-effect of hydrostatic pressure appears to play a greater role and slows down the temperature-induced expansion of the FVEs [23]. To interpret the behavior of I_3, it is important to note that in the rubbery phase there exist only *dynamic* FVEs, whereas in the glassy phase also *static* FVEs can exist due to the non-equilibrium nature of that phase. The decrease in I_3 and the simultaneous increase in I_2 at lower temperatures (cfr. Fig. 8) was explained by the creation of additional smaller holes, which act as positron traps [44]. Another possible explanation of this phenomenon can be made by applying the dual-mode sorption model [12,45–47]. According to this model the gas transport in the glassy polymer is governed by two competing modes:

In the first mode the gas dissolves in the polymer matrix, while in the second mode the gas adsorbs in the *static* FVEs and can get immobilized there [12,47]. With increasing pressure, the number of gas atoms that can be trapped by the *static* FVEs also increases, obscuring more *static* FVEs for o-Ps pick-up annihilation. This is reflected in Fig. 7 for 0.1 MPa, 2 MPa and 4 MPa below 75 °C. The positrons that are not forming positronium, due to the decrease in vacant *static* FVEs, will eventually annihilate in the polymer matrix, contributing to I_2, which can be seen in Fig. 8. Furthermore, the second mode is temperature dependent and should diminish as the *static* FVEs and gas atoms become more mobile with temperature and convert to a more dynamic state. The temperature dependence can be seen in Figs. 7 and 8. Since the average size of the FVEs and the size of gas atoms are in the same order of magnitude, the occupation of the *static* FVEs seems to only have an effect on the amount ($\sim I_3$) and not on the size of the FVEs ($\sim\tau_3$). Under vacuum conditions, gas atoms are removed from the polymer, resulting in less plasticization. In the glassy phase, an overall reduction in V_F is visible, which is probably due to the rigid chains imploding and hence, closing some of the FVEs. Transitioning to the rubbery phase, the polymer matrix reaches an equilibrium state and the chains can relax, forming new *dynamic* FVEs. This is reflected in the rapid increase of I_3 at the phase transition.

One possible reason why the intensity of the vacuum measurement is highest above the T_g may be that there are no argon atoms to occupy some of the *dynamic* FVEs, as is the case with the pressurized material. Please note that this is the first test measurement to show the potential of measuring PALS on soft matter materials with simultaneously controlling pressure, atmosphere composition and temperature, a more detailed investigation is needed to fully elucidate the occurring phenomena. Note that these effects can change for other gas species and polymers [23].

4. Summary and conclusion

In this paper, we present proof of concept for an apparatus that allows us to measure positron lifetime spectra as a function of temperature, gas pressure, and atmospheric composition. The technical description of the system and the exact specifications have been defined. The samples can be heated up to 200 °C or be exposed to vacuum or a desired gas atmosphere of up to 20 MPa. Moreover, a combined treatment with temperature and pressure at slightly reduced values (see Fig. 1b) are also possible. The ability to control all three parameters simultaneously in this parameter range during the measurement is unique to date. The application of the instrument was demonstrated by using PS as an example. Here, the effect of temperature and argon atmosphere on the V_F of the polymer was investigated (see Table 1). It was shown that the size of the FVEs is a function of the argon pressure and sample temperature and can be explained by the plasticization of the polymer matrix. In addition, an alternative explanation of the temperature and pressure dependent reduction of I_3 below the T_g was given. The results are compared to the results of investigations on polystyrene or other polymer systems where either atmosphere, pressure or temperature was varied but never simultaneously [21–24]. Overall, the test measurements on Polystyrene show the capability of the in-situ multi-parameter control during PALS for the investigation of polymer material. A more detailed investigation of the evolution of the V_F of PS under different gas atmospheres will be performed in future experiments with the instrument introduced in this work. Also, in more applied fields of science, the instrument could be useful for in-situ measurements; e.g., to analyze the behavior of a gas separation membrane upon contact with gasses, to follow-up the vapor-induced crosslinking degree of a polymer, or to investigate the behavior of different adsorbents for air remediation.

CRediT authorship contribution statement

R. Helm: Writing – review & editing, Writing – original draft, Formal analysis. **J. Lehtonen:** Methodology, Investigation. **M. Mayerhofer:** Writing – review & editing, Validation. **J. Mitteneder:** Resources. **W. Egger:** Validation. **R. Verbeke:** Writing – review & editing, Writing – original draft. **P. Sperr:** Methodology, Conceptualization. **G. Dollinger:** Writing – original draft. **M. Dickmann:** Project administration, Conceptualization.

Declaration of competing interest

The authors declare that they have no known competing financial interests or personal relationships that could have appeared to influence the work reported in this paper.

Data availability

Data will be made available on request.

Acknowledgments

The authors would like to thank L. Hackel and R. Schubert for supporting this work by fabricating the parts for the instrument. Furthermore, the authors thank S. Girst for proofreading. In addition, the authors acknowledge the financial support by the University of the Bundeswehr Munich.

References

[1] P. Bernardo, E. Drioli, G. Golemme, Membrane gas separation: A review/state of the art, Ind. Eng. Chem. Res. 48 (10) (2009) 4638–4663.
[2] R.W. Baker, Future directions of membrane gas separation technology, Ind. Eng. Chem. Res. 41 (6) (2002) 1393–1411.
[3] K. Sumida, D.L. Rogow, J.A. Mason, T.M. McDonald, E.D. Bloch, Z.R. Herm, T.-H. Bae, J.R. Long, Carbon dioxide capture in metal-organic frameworks, Chem. Rev. 112 (2) (2012) 724–781.
[4] L. Ma, L. Gutierrez, R. Verbeke, A. D'Haese, M. Waqas, M. Dickmann, R. Helm, I. Vankelecom, A. Verliefde, E. Cornelissen, Transport of organic solutes in ion-exchange membranes: mechanisms and influence of solvent ionic composition, Water Res. 190 (2021) 116756.
[5] K. Hanaki, Water-quality Engineering, Elsevier, Amsterdam, 2011.
[6] M. Elimelech, W.A. Phillip, The future of seawater desalination: energy, technology, and the environment, Science 333 (6043) (2011) 712–717.
[7] C.A. Angell, Glass Formation and the Nature of the Glass Transition, in Insulating and Semiconducting Glasses (Series on Directions in Condensed Matter Physics) (ed P. Boolchand), World Scientific, 2000, pp. 1–51.
[8] J.S. Vrentas, J.L. Duda, Diffusion in polymer—solvent systems. I. Reexamination of the free-volume theory, J. Polym. Sci. Polym. Phys. Ed. 15 (3) (1977) 403–416.
[9] H. Eyring, Viscosity, plasticity, and diffusion as examples of absolute reaction rates, J. Chem. Phys. 4 (4) (1936) 283–291.
[10] K. Ganesh, R. Nagarajan, J.L. Duda, Rate of gas transport in glassy polymers: a free volume based predictive model, Ind. Eng. Chem. Res. 31 (3) (1992) 746–755.
[11] R.P. White, J.E.G. Lipson, Polymer free volume and its connection to the glass transition, Macromolecules 49 (11) (2016) 3987–4007.
[12] S. Zhou, S.A. Stern, The effect of plasticization on the transport of gases in and through glassy polymers, J. Polym. Sci. B Polym. Phys. 27 (2) (1989) 205–222.
[13] A.E. Hamielec, M. Eldrup, O. Mogensen, Positron annihilation techniques (PAT) in polymer science and engineering, J. Macromol. Sci., Part C 9 (2) (1973) 305–337.
[14] Y.C. Jean, Positron annihilation spectroscopy for chemical analysis: A novel probe for microstructural analysis of polymers, Microchem. J. 42 (1) (1990) 72–102.
[15] W. Brandt, S. Berko, W.W. Walker, Positronium decay in molecular substances, Phys. Rev. 120 (4) (1960) 1289–1295.

[16] R.E. Bell, R.L. Graham, Time distribution of positron annihilation in liquids and solids, Phys. Rev. 90 (4) (1953) 644–654.
[17] R.A. Ferrell, Theory of positron annihilation in solids, Rev. Mod. Phys. 28 (3) (1956) 308–337.
[18] Y.C. Jean, J.D. van Horn, W.-S. Hung, K.-R. Lee, Perspective of positron annihilation spectroscopy in polymers, Macromolecules 46 (18) (2013) 7133–7145.
[19] D. Lightbody, J.N. Sherwood, M. Eldrup, Vacancy formation energies in plastic crystals using positron annihilation techniques, Mol. Cryst. Liq. Cryst. 96 (1) (1983) 197–210.
[20] A. Uedono, T. Kawano, S. Tanigawa, M. Ban, M. Kyoto, T. Uozumi, Transition and relaxation processes of polyethylene, polypropylene, and polystyrene studied by positron annihilation, J. Polym. Sci. B 35 (10) (1997) 1601–1609.
[21] J. Liu, Q. Deng, Y.C. Jean, Free-volume distributions of polystyrene probed by positron annihilation: comparison with free-volume theories, Macromolecules 26 (26) (1993) 7149–7155.
[22] Y.C. Jean, J. Zhang, H. Chen, Y. Li, G. Liu, Positron annihilation spectroscopy for surface and interface studies in nanoscale polymeric films, Spectrochim. Acta A Mol. Biomol. Spectrosc. 61 (7) (2005) 1683–1691.
[23] X. Hong, Y.C. Jean, H. Yang, S.S. Jordan, W.J. Koros, Free-volume hole properties of gas-exposed polycarbonate studied by positron annihilation lifetime spectroscopy, Macromolecules 29 (24) (1996) 7859–7864.
[24] Jürgen Pionteck, Muhamad Qasim Shaikh, Liane Häußler, Stefan Thränert, E. M. Hassan, Reinhard Krause-Rehberg (1244) https://www.degruyter.com/document/doi/10.1515/epoly.2007.7.1.1244/xml. e-Polymers (1).
[25] ANSYS, Inc. (2023) ANSYS 2023 R1.
[26] Dassault Systems (2022) SolidWorks.
[27] HAMAMATSU Photonics K.K Photomulitplier Tubes R13478, R13449, R13408, R13089, R15608. https://www.hamamatsu.com/eu/en/product/optical-sensors/pmt.html.
[28] DRS4 evaluation board (2014).
[29] R. An, B. Chen, Y.-F. Liu, B.-J. Ye, W. Kong, S. Ritt, A new positron annihilation lifetime spectrometer based on DRS4 waveform digitizing board, Chinese Phys. C 38 (5) (2014) 56001.
[30] M. Petriska, S. Sojak, V. Slugeň, Positron lifetime setup based on DRS4 evaluation board, J. Phys.: Conf. Ser. 505 (2014) 12044.
[31] D. Petschke, T.E. Staab, DDRS4PALS: A software for the acquisition and simulation of lifetime spectra using the DRS4 evaluation board, SoftwareX 10 (2019) 100261.
[32] R. Krause-Rehberg, H.S. Leipner, Positron annihilation in semiconductors: Defect studies; with 20 tables, 2nd ed., Springer, Berlin, 2003.
[33] H. Eslami, F. Müller-Plathe, Molecular dynamics simulation of sorption of gases in polystyrene, Macromolecules 40 (17) (2007) 6413–6421.
[34] F. Mozaffari, H. Eslami, J. Moghadasi, Molecular dynamics simulation of diffusion and permeation of gases in polystyrene, Polymer 51 (1) (2010) 300–307.
[35] A.R. Berens, H.B. Hopfenberg, Diffusion of organic vapors at low concentrations in glassy PVC, polystyrene, and PMMA, J. Membr. Sci. 10 (2–3) (1982) 283–303.
[36] V. Teplyakov, P. Meares, Correlation aspects of the selective gas permeabilities of polymeric materials and membranes, Gas Sep. Purif. 4 (2) (1990) 66–74.
[37] S.J. Tao, Positronium annihilation in molecular substances, J. Chem. Phys. 56 (11) (1972) 5499–5510.
[38] M. Eldrup, D. Lightbody, J.N. Sherwood, The temperature dependence of positron lifetimes in solid pivalic acid, Chem. Phys. 63 (1–2) (1981) 51–58.
[39] K. Ito, H. Nakanishi, Y. Ujihira, Extension of the equation for the annihilation lifetime of ortho-positronium at a cavity larger than 1 nm in radius, J. Phys. Chem. B 103 (21) (1999) 4555–4558.
[40] C.L. Choy, Thermal conductivity of polymers, Polymer 18 (10) (1977) 984–1004.
[41] H.-L. Li, Y. Ujihira, A. Nanasawa, Y.C. Jean, Estimation of free volume in polystyrene-polyphenylene ether blend probed by the positron annihilation lifetime technique, Polymer 40 (2) (1999) 349–355.
[42] R.A. Assink, Plasticization of poly(dimethyl siloxane) by high-pressure gases as studied by NMR relaxation, J. Polym. Sci. Polym. Phys. Ed. 12 (11) (1974) 2281–2290.
[43] Y. Kamiya, K. Mizoguchi, Y. Naito, A dielectric relaxation study of plasticization of poly(ethyl methacrylate) by carbon dioxide, J. Polym. Sci. B 28 (11) (1990) 1955–1964.
[44] Z. Yu, U. Yahsi, J.D. McGervey, A.M. Jamieson, R. Simha, Molecular weight-dependence of free volume in polystyrene studied by positron annihilation measurements, J. Polym. Sci. B 32 (16) (1994) 2637–2644.
[45] D.R. Paul, Gas sorption and transport in glassy polymers, Ber. Bunsen. Phys. Chem. 83 (4) (1979) 294–302.
[46] R.M. Barrer, Diffusivities in glassy polymers for the dual mode sorption model, J. Membr. Sci. 18 (1984) 25–35.
[47] J. Guo, T.A. Barbari, Unified dual mode description of small molecule sorption and desorption kinetics in a glassy polymer, Macromolecules 42 (15) (2009) 5700–5708.